EFDA–JET–PR(08)08

S. Saarelma, A. Alfier, M.N.A Beurskens, R. Coelho, I. Nunes,
H.R. Koslowski, Y. Liang, and JET EFDA contributors

MHD Stability Analysis of Small ELM Regimes in JET

MHD Stability Analysis of Small ELM Regimes in JET

S. Saarelma[1], A. Alfier[2], M.N.A. Beurskens[1], R. Coelho[3], I. Nunes[3], H.R. Koslowski[4], Y. Liang[4], and JET EFDA contributors*

JET-EFDA, Culham Science Centre, OX14 3DB, Abingdon, UK

[1]EURATOM-UKAEA Fusion Association, Culham Science Centre, OX14 3DB, Abingdon, OXON, UK
[2]Associazione EURATOM-ENEA sulla Fusione, Consorzio RFX Padova, Italy
[3]Centro de Fuso Nuclear, Associao EURATOM-IST, Lisboa, Portugal
[4]Forschungszentrum Jülich GmbH, Association EURATOM-FZ Jülich, Institut für Plasmaphysik, Trilateral Euregio Cluster, D-52425 Jülich, Germany
** See annex of M.L. Watkins et al, "Overview of JET Results ", (Proc. 21 st IAEA Fusion Energy Conference, Chengdu, China (2006)).*

Preprint of Paper to be submitted for publication in
Plasma Physics and Controlled Fusion

ABSTRACT.
We have analysed the edge stability of JET discharges with small ELMs using the high resolution Thomson scattering system for accurate edge profiles in the equilibrium reconstruction. For the reference plasmas with large Type I ELMs we confirm the results from earlier analyses that the edge stability is limited by intermediate-n peeling-ballooning modes with a relatively large radial extent. The double null configuration needed to replace Type I ELMs by smaller Type II ELMs greatly increases the stability against these modes while the stability against n = ∞ ballooning modes is not affected. When this is combined with high collisionality (which is the other requirement for Type II ELMs), we find that the plasma can not reach the Type I ELM triggering peeling-ballooning mode stability boundary before it is destabilised by high-n ballooning modes resulting in more benign ELMs. The ELM mitigation by magnetic perturbation causes the edge stability to be limited by pure peeling modes with a narrow radial extent. This explains the smaller ELM size and also why the ELMs are not fully suppressed. The transition from Type I ELMs to Type III ELMs by increasing the edge radiation fully stabilises the edge plasma against ideal MHD modes. Therefore, the Type III ELMs are due to be triggered by some other mechanism than an ideal MHD instability.

1. INTRODUCTION

The High-confinement-mode (H-mode) in present day tokamaks is regularly accompanied by Edge Localized Modes (ELMs) which can create high heat loads on the divertor plates. While current tokamaks can sustain these loads they may lead to intolerable divertor erosion in future tokamak fusion reactors. For instance, the prediction for the ITER base line H-mode is that unmitigated Type I ELM losses are well above the tolerable level [1]. Therefore, it's important to develop operating scenarios or control techniques where large ELM losses are avoided.

Such operating regimes can be passive, i.e. ELMs become small due to the chosen plasma conditions. Small or no ELMs have been achieved in Quiescent H-mode [2, 3], enhanced D regime [4, 5] or Type II ELMs [6, 7, 8, 9]. It is also possible to actively perturb the edge plasma leading to either increased edge transport or small and frequent ELMs, thus avoiding the large ELMs with high heat losses. These methods include giving plasma vertical "kicks"[10], injecting small pellets into the plasma [11], injecting impurities into the plasma [12] and ergodising the plasma edge using external coils [13].

The large Type I ELMs are generally believed to be triggered when the plasma edge region crosses the ideal peeling-ballooning mode stability boundary [14]. In order to understand why the ELMs are either completely absent or the size of the ELMs is reduced, one can compare the edge stability in plasmas with small or no ELMs with the plasmas showing large Type I ELMs.

In this paper, we investigate the edge stability of JET plasmas in Type II ELMy conditions, during impurity injections and with magnetic perturbations from external Error Field Correction Coils (EFCC). The recent installation of a High Resolution Thomson Scattering (HRTS) system in

JET has greatly improved the accuracy of edge profile measurements, thus improving the accuracy of stability analysis.

The JET plasmas that are chosen for stability analysis are all characterised by the absence of large Type I ELMs. The edge stability of these plasmas is compared with reference plasmas with Type I ELMs. The changes in the ELM behaviour can be explained by the changes in the edge stability properties.

2. EXPERIMENTAL PLASMAS

We investigate three types of small ELM regimes, Type II ELMs in quasi doublenull conditions, ELM mitigation by impurity injection and ELM mitigation by edge ergodisation. These plasmas are very different from each other. Therfore, the elimination of large Type I ELMs is unlikely to be caused by the same mechanism in all cases.

2.1. TYPE II ELMS

Type II ELMs have been observed in many devices earlier [9, 7, 6]. In JET, the requirements for Type II ELMs are high density ($n_{ped}/n_{GW} > 0.7$) and almost double null configuration [15, 16]. In these conditions large Type I ELMs are replaced by small Type II ELMs without degradation of plasma confinement as happens with Type III ELMs. Figure 1 shows the D_α signal of a high density double null discharge and a reference single null Type I ELM discharge. The global parameters in the investigated double-null discharge (Pulse No: 70500) studied in this paper are I_p = 0.86MA, B_t = 1.2T and total heating power of 9MW. The H-factor ($H98_{(y,2)}$) is about 1.0 and equal to the reference Type I ELM discharge.

2.2. ELM MITIGATION USING MAGNETIC PERTURBATION

The method of suppressing large Type I ELMs using edge ergodisation with internal coils was first used in DIII-D [13]. Since then ELM mitigation using magnetic perturbations has also been successfully used in TEXTOR [17]. Also in JET ELMs have been mitigated using Error Field Correction Coils (EFCC) in n = 1 mode [18]. Unlike in DIII-D, the edge ergodisation has not lead to a complete suppression of ELMs but instead the ELM size is reduced and the frequency increased. Figure 2 shows how the peaks in the D_α signal become smaller during the EFCC operation. Similarly, the plasma energy loss and the pedestal temperature drop during an ELM are also reduced during the EFCC [19].

During the EFCC operation, the pedestal temperature remains at the pre-EFCC level. Pedestal density, on the other hand, is significantly reduced. The resulting pedestal pressure gradient is reduced by up to 20% during the mitigation [19]. However, the pressure pedestal height stays almost constant throughout the EFCC phase. In addition to the pedestal effects, the plasma rotation is globally reduced by the EFCC.

The pedestal position also moves radially inwards during the EFCC operation. While this shift is

clearly visible in real space (R, z), the shift can actually be due to the slight kinking of the plasma caused by the n = 1 perturbation as well as shrinking due to the feedback response from the shape control. Thus, it is not clear if the profiles shift with respect to the plasma boundary or the entire plasma shifts and shrinks. In the modeling we have assumed that the relative position of the profiles with respect to the separatrix does not change with EFCC operation, but take into account the changed plasma size. In addition to the shrinking due to the feedback system, the n = 1 magnetic perturbation also kinks the plasma [20]. Therefore, strictly speaking the plasma is no longer axisymmetric. However, since the asymmetric perturbation of the plasma outer surface is only about 0.3% of the normalised flux [19], we can assume that this has very little effect on the stability and use axisymmetric codes for equilibrium and stability calculations.

2.3. ELMS IN HIGHLY RADIATING PLASMA

Injecting impurities into the plasma has been an easy way to affect ELM behaviour [21]. In JET nitrogen seeding experiments, the large Type I ELMs are first replaced by smaller Type III ELMs and eventually by L-mode as the edge radiation fraction (F_{rad}) is increased. The D_α signal of F_{rad} = 15% (Pulse No: 70355), F_{rad} = 45% (Pulse No: 70281) and F_{rad} = 62% (Pulse No: 70289) are shown in Fig.3. These discharges had high triangularity (δ = 0.4) and global parameters were I_p = 1.9MA and B_t = 3.1T and total heating power of 20-25MW. As usual for non-ITB plasmas, the global confinement is degraded by the transition to Type III ELMs and then even more as the plasma loses H-mode. A more detailed description of the experiment can be found in [22].

3. EDGE STABILITY ANALYSIS

ELMs are generally believed to be triggered by MHD instabilities near the plasma edge [23, 24]. Therefore, to gain understanding of the changes in ELM behaviour observed in experiments, we need to investigate how the plasma stability properties near the edge have changed.

For stability analysis of the edge plasma we create an equilibrium matching the actual plasma as closely as possible. Then we perturb the equilibrium from this socalled operational point by varying the pressure gradient and current density in the edge region. This is done by multiplying the current density and/or pressure gradient with a Gaussian function that is centered in the middle of the pedestal and has the same width as the pedestal. In this way both profiles stay continuous unlike if the profiles were multiplied by a step function for instance. We determine the stability of each of the new equilibria, thus mapping the stability boundaries in the vicinity of the operational point in normalised pressure gradient (α) edge current density (j) space. The definition of α used in this paper is [25]:

$$\alpha = \frac{-2\delta V/\delta y}{(2\pi)^2}\left(\frac{V}{2\pi^2 R_0}\right)^{1/2}\mu_0\frac{\delta p}{\delta \psi}, \qquad (1)$$

where V is the volume enclosed by the flux surface, R_0 is the geometric centre of the plasma and ψ

is the poloidal flux.

Most of the points in the stability diagram are naturally unrealistic for real plasmas, i.e. the equilibrium current density is not consistent with the bootstrap current corresponding to the pressure gradient value. Therefore, in addition to the stability boundaries, in some cases we calculate a self-consistent “path” in the diagram for the experimental equilibrium by varying the density and temperature profiles and calculating the corresponding current profile. Moving along this path represents the build up of the pressure pedestal before an ELM.

To interpret the stability calculation results we use the constructed stability diagram and the nature of the identified instabilities (mode numbers, shape of the eigenfunction) on the self-consistent path of the experimental plasma for explaining the observed ELM behaviour.

The HRTS system in JET allows an accurate determination of the edge electron density and temperature profiles. In the equilibrium reconstruction we assume that $T_i = T_e$. It must be noted that this assumption can overestimate the steepness of the edge ion temperature gradient. Using these profiles, we calculate the bootstrap current (that dominates in the edge region) self-consistently with an analytical formula [26]. In addition to the bootstrap current we assume that the inductive current is distributed as the conductivity profile, i.e. we assume that the current is fully diffused. This might produce an error in the core current profile, but since we are interested in the edge stability, it has no effect on the results presented here. The amplitude of the inductively driven current is adjusted so that the total current of the equilibrium matches with the experiment. Figure 4 shows the flux surface averaged toroidal current and q-profiles of a typical reconstruction of a Type I ELM equilibrium.

The shape of the plasma is taken from EFIT[27]. However, since we use the fixed boundary equilibrium code HELENA [28] that can not handle a true X-point, we have to modify the boundary shape slightly near the X-point. The rounding of the X-point makes little difference for the peeling-ballooning or pure ballooning mode stability, but the growth rate of pure peeling modes can be affected by it. However, since the peeling modes here are driven by the finite edge current and not by the current density gradient near the edge, the actual stability boundary (at what current and pressure gradient the mode becomes unstable) should not be affected by the X-point treatment [29].

For the equilibrium reconstruction using HELENA we need both the pressure and current profiles in poloidal flux space (ψ). While the profiles obtained from the HRTS system fix them very accurately in real space (R, z), they can often be slightly offset in poloidal flux space obtained from EFIT, due to the errors in mapping. We correct this by assuming that separatrix electron temperature is in the range of 100-200eV based on power balance calculations in JET H-mode discharges [30]. The required radial shifts are of order of 2% in poloidal flux corresponding to about 1cm on the outer midplane. Using the radial shifts on profiles eliminates the stability effects due to unrealistic separatrix temperatures, e.g. peeling modes triggered by the very high edge current driven by the low resistivity in high temperature. While the stability boundaries are to some extent sensitive to the separatrix position, the given range of realistic separatrix temperatures fixes the pedestal position so well (< 1%

of poloidal flux) that this effect is quite small. Also the mode that becomes unstable first does not change with small radial shifts of the profiles.

The stability of the created equilibria is studied using the ideal MHD stability code ELITE[31, 32]. While ELITE can not solve for very low toroidal mode number, such as n = 1 modes, we have been able to use it down to n = 3. In cases where ELITE found the stability boundary been set by the n = 3 mode (a pure peeling mode), we have recalculated the stability for n = 1–3 using MISHKA-1 code [33]. We found that while in many cases also n = 1 and n = 2 modes were unstable, indeed n = 3 is the most unstable mode. The highest toroidal mode numbers routinely investigated was n = 25. In the cases were the stability boundary closest to the operational point was set by the high-n modes, we complemented the ELITE analysis for finite n with the standard n = ∞ ballooning mode analysis in the HELENA code.

We have used a criterion for an unstable mode $\gamma/\gamma_A > 0.001$, where is the growth rate of the mode and γ_A is the Alfvén frequency. This is quite a relaxed criterion that only leaves out the marginally unstable modes. Using a more stringent criterion such as $\gamma > \omega_{*,i},/2$ [14], where $\omega_{*,i}$ is the ion diamagnetic frequency would make the stable region slightly larger. While in some cases this could make the experimental point to change from unstable to stable, it is unlikely to change the qualitative result, i.e. which stability limit the plasma crosses and which mode becomes unstable first.

3.1. TYPE II ELMS

Experimentally there are two required condition for accessing Type II ELMs in JET. The plasma has to be almost double null and the edge plasma must have high collisionality ($v_* > 0.32$) [16]. We test the effect of both the plasma shape and the edge collisionality on the stability. For the shape study, we take the plasma profiles (shown in Fig.5) from a Type II ELMy Pulse No: 70500 and use them for both the actual Pulse No: 70500 shape and the shape of a similar single null Pulse No: 69147. Since the plasma profiles are now identical, all the differences in the stability properties must be due to the plasma shape. Figure 6 shows the shapes of the investigated plasmas. As can be seen, the triangularity of single and double null plasmas are quite similar and the main difference in shape is the slight elongation in the double null plasma near the second X-point.

Using the measured temperature and density profiles of Pulse No: 70500 and calculated self-consistent bootstrap current we create the operational point equilibria for single and double null plasmas. The q-profiles of these equilibria are plotted in Fig.7. As expected, the q-profiles match perfectly in the plasma core where the boundary shape has little effect. However, near the edge the magnetic shear s = (dq/dr)/(q/r) is much stronger in the double null plasma due to the effect of the second X-point.

The relatively small changes to the equilibrium have quite large effects on the edge stability. Figure 8 shows the stability diagram of the single null and double null plasmas. The main difference is that the intermediate-n stability boundary, i.e. the upper right corner, has expanded to higher

values of α and j_{edge} with the inclusion of the second X-point. Due to this shift of stability boundary, the operational point (the equilibrium corresponding experimental profiles) is unstable for single null plasma shape while it is stable for the double null shape. On the other hand, the high-n ballooning boundary (the limit for pressure gradient at low values of edge current) has remained more or less unchanged.

We have also plotted in Fig.8 how the operational point changes if we keep the edge pressure gradient constant, but increase temperature and decrease density or vice versa. As expected, α does not change, but the edge current increases with high temperature and low density and decreases with low temperature and high density. This is mainly due to the increased edge collisionality. This means that a plasma with high edge density and low edge temperature is going to hit the stability boundary set by the high–n ballooning modes instead of intermediate–n peeling-ballooning modes. This is true especially for the double null plasma because its peeling-ballooning mode boundary is significantly expanded into higher values of α from that of the single null plasma.

Combining the two effects (improved stability against Type I ELM triggering peeling-ballooning modes in double null plasma and moving the operational point closer to the ballooning mode with high density and low temperature) allows us to conclude that in Type II ELM plasmas the intermediate-n peeling-ballooning modes are avoided and ELMs are triggered by high-n ballooning modes instead. The reduction in ELM size is probably due to the fact that high-n ballooning mode boundary is more like a “soft” boundary than the peeling-ballooning boundary in the upper right corner of α–j diagram. When the operational point reaches the ballooning boundary, the resulting instability relaxes the pressure gradient and it immediately returns the plasma back to the stable region. In the peeling-ballooning boundary, unstable plasma has to have its edge current reduced before it can become stable again.

3.2. ELM MITIGATION USING MAGNETIC PERTURBATION

For the stability analysis of ELM mitigation by application of magnetic perturbation we choose JET Pulse No: 69557. In order to get insight on why the ELM behaviour changes during EFCC operation, we analyse the edge stability of the plasma both during the Type I ELM phase (18.463s) of the discharge and during the mitigation phase (19.263s). The electron density, temperature and pressure profiles at these time points are shown in Fig.9. As can be seen the density pedestal is reduced and temperature pedestal maintained during the EFCC operation. Consequently, the pressure gradient is about 20% lower during the EFCC phase.

Figure 10 shows the stability boundaries for the Type I and mitigated phase and Figure 11 the radial mode structure of the most unstable mode in the experimental point, i.e. just after crossing the stability boundary along the plotted “path”. The ELM mitigation using EFCC changes the ELM triggering instability from intermediaten peeling-ballooning mode that is driven by both the current density and the pressure gradient into a low-n peeling mode that is driven only by the current density.

At the same time the width of most unstable mode decreases. Figure 12 shows the width of the

most unstable mode along a path with increasing density and temperature gradients and self-consistent bootstrap current (black lines in Fig.10). In the Type I ELM phase the width of the mode "jumps" straight to 3% of the poloidal flux as the plasma crosses the stability boundary while during the application of magnetic perturbation the mode width grows gradually from almost zero as the stability boundary is crossed, i.e. the width of the marginally unstable mode is very narrow. In addition, the pure peeling-mode peaks at the plasma boundary while a peeling-ballooning mode has a peak inside the plasma. Assuming that the eigenfunction width of the ELM triggering instability and the location of the mode maximum affects the ELM size (the width of the temperature perturbation due to an ELM is shown to match the eigenfunction of the most unstable mode on DIII-D [14]), the stability analysis results can explain why the ELM size is reduced during the ELM mitigation phase. Also as explained in [34] just the switch to low-n peeling mode from the intermediate-n peeling-ballooning mode can make the unstable mode to saturate faster, thus leading to smaller ELM losses.

The main difference in ELM suppression in JET using magnetic perturbation compared with a similar experiment in DIII-D [13] was that unlike in DIII-D, the ELMs were not fully suppressed in JET. In DIII-D the operational point moves into the stable region during the application of the magnetic perturbation [35]. As shown above, also in JET the operational point moves, but is still limited by a peeling mode stability boundary. Therefore, the ELMs are not completely eliminated, but only get smaller.

During the EFCC operation the toroidal rotation exhibits strong braking. For the edge this means that the rotation shear decreases [18]. It has been shown that in tight aspect ratio tokamak MAST, the edge rotation shear can significantly affect the edge stability [36]. However, for JET plasmas the ELITE modelling yields that the stabilising effect of the rotation shear is minimal. Only the marginally unstable equilibria can be stabilised by placing a sheared rotation at the pedestal region. The difference to MAST is due to two effects. Firstly, the stabilising effect of the rotation is stronger in tight aspect ratio plasma. Secondly, MAST is rotating faster (with respect to the Alfvén time) than JET. Since the rotation effects are minimal, the stability boundaries are not affected by them (in figures showed in this paper, the boundaries would move less than the distance between two equilibrium points) and it is also unlikely that the flattened rotation profile during the EFCC operation plays an important role explaining the observed ELM mitigation.

3.3. EDGE STABILITY IN HIGHLY RADIATING PLASMAS

The edge profiles of the impurity seeding experiment are shown in Fig.13. The profiles are averaged over several laser pulses to gain good statistics, thus reducing error. The large difference in edge pressure gradients between these discharges leads to large differences in calculated edge bootstrap current profiles as shown in Fig.14 where the flux surface averaged toroidal current is plotted as a function of poloidal flux. Also the high value of Z_{eff} in high radiation discharges reduces the bootstrap current.

The low edge pressure gradient and current density in Type III ELMy and L-mode discharges makes them also stable against ideal edge instabilities. Figure 15 depicts in one stability diagram all three discharges. As expected the Type I ELMy (Pulse No: 70355) is just at the stability boundary against peeling-ballooning modes. The Type III ELMy (Pulse No: 70281) is far from both the low-n peeling and high-n ballooning modes. Therefore, it is unlikely that the ELMs in this discharge are triggered by ideal modes. This agrees with earlier study of Type III ELMs in JET [37]. In this paper we did not investigate resistive modes that could become unstable even if the plasma is ideally stable. The L-mode (Pulse No: 70289) is even further away from any stability limits. In this case, the edge pressure gradient is more likely to be limited by transport than any MHD stability limit.

CONCLUSIONS

We have shown how the ideal stability properties of the edge plasma behave in three small ELM regimes, Type II ELMs, EFCC ELM mitigation and highly radiating plasmas. Even though in every case large Type I ELMs are replaced by smaller ELMs, the edge stability in each case is quite different from the others.

In Type II ELM plasmas the double null configuration greatly expands the stable region in the upper-right corner of the $\alpha-j$ diagram while keeping the high-n ballooning stability virtually unchanged. When this is connected with the Type II ELM requirement of high density and low temperature, it means that the Type II ELMy edge plasma avoids the dangerous intermediate-n peeling-ballooning modes that trigger Type I ELMs and are instead limited by the more benign high-n ballooning modes.

During the Type I ELMy phase before the EFCC mitigation, the edge plasma is, as expected, in the upper-right corner of the stability diagram with a wide intermediate-n peeling-ballooning mode as the most unstable instability. During the mitigation by an $n = 1$ perturbation magnetic field the operational point moves to the peeling limit of the stability diagram. The most unstable mode becomes a narrow low-n mode. The narrow width of the mode can explain why the ELM size is reduced during the EFCC operation. Unlike in DIII-D, during the EFCC operation in JET the edge stability is still limited by an ideal mode. Consequently the ELMs are not fully suppressed. The impurity seeded transition from Type I ELMs to first Type III ELMs and then to L-mode is seen as a complete separation of ideal MHD stability boundary in the plasma edge region. The resulting Type III ELMs are likely to be triggered by some other mechanism, such as resistive modes.

ACKNOWLEDGMENTS

This work was partly funded by Euratom and the UK Engineering and Physical Sciences Research Council. The views and opinions expressed herein do not necessarily reflect those of the EuropeanCommission. This work was carried out within the framework of the European Fusion Development Agreement. The authors would like to thank P.B. Snyder and H.R. Wilson for the support on the ELITE code issues.

REFERENCES

[1]. Loarte A. et al.; Power and particle control, Nucl. Fusion **47** (2007) S203.
[2]. Burrell, K.H. et al., Plasma Phys. and Contr. Fusion, **44** (2002), A253.
[3]. Suttrop, W., et al., Plasma Phys. Control. Fusion **45** (2003) 1399.
[4]. Takase, Y., et al., Phys. of Plasmas, **4** (1997) 1647.
[5]. Hubbard, A.E., et al., Phys. of Plasmas, **8** (2001) 2033.
[6]. Ozeki, T. et al., Nuclear Fusion **30** (1990) 1425.
[7]. Kamada, Y. et al., Plasma Phys. and Contr. Fusion, **42** (2000) A247.
[8]. Kamada, Y. et al, Plasma Phys. and Contr. Fusion, **38** (1996) 1387.
[9]. Stober, J. et al, Nucl. Fusion **41** (2001) 1123.
[10]. Degeling, A.W., et al., Plasma Phys. and Contr. Fusion, **45** (2003) 1637.
[11]. Lang, P.T., et al., Nuclear Fusion **43** (2003) 1110.
[12]. Maddison, G.P. et al., Plasma Phys. Control. Fusion **45** (2003) 1657.
[13]. Evans T.E. et al, Phys. Rev. Lett. **92** (2004) 235003.
[14]. Snyder, P.B. et al., Phys. of Plasmas **9** (2002) 2037.
[15]. Saibene G., et al, Nucl. Fusion **45** (2005) 297.
[16]. Nunes I., et al, 34th EPS Conf. on Controlled Fusion and Plasma Physics, Warsaw, Poland (2007).
[17]. Finken K.H. et al., Nucl. Fusion **47** (2007) 522.
[18]. Liang Y., et al., Phys. Rev. Lett. **98**, 265004 (2007).
[19]. Alfier A., et al. submitted to Nucl. Fusion.
[20]. Chapman I.T. et al, Nucl. Fusion **47** (2007) L36.
[21]. Jachmich S., et al, Plasma Phys. and Contr. Fusion **44** (2002) 1879.
[22]. Beurskens M.N.A, et al., submitted to Nucl. Fusion.
[23]. Huysmans G.T.A, Plasma Phys. and Contr. Fusion **47** (2005) B165.
[24]. Snyder P.B., et al., Nucl. Fusion **44** (2004) 320.
[25]. Miller R.L., et al., Phys. of Plasma **5** (1998) 973.
[26]. Sauter O., C. Angioni, Y.R. Lin-Liu, Phys. of Plasmas, **6** (1999) 2834.
[27]. Lao L., et al, Nucl. Fusion **25** (1985) 1611.
[28]. Huysmans G.T.A., Goedbloed J.P., Kerner W.O.K., Computational Physics (Proc. Int. Conf. Amsterdam, 1991),World Scientific Publishing, Singapore (1991) 371.
[29]. Huysmans G.T.A, Plasma Phys. and Contr. Fusion **47** (2005) 2107.
[30]. Kallenbach A. et al., Plasma Phys. and Contr. Fusion **46** (2004) 431.
[31]. Wilson H.R., Snyder P.B., Huysmans G.T.A. and Miller R.L., Phys. Plasmas **9** (2002) 1277.
[32]. Snyder P.B., Wilson H.R., et al., Phys. Plasmas **9** (2002) 2037.
[33]. Mihailovskii A.B., et al., Plasma Phys. Rep. **23** (1997) 844.
[34]. Snyder P.B. et al., Nucl. Fusion **47** (2007) 961.
[35]. Evans T.E. et al. Plasma Phys. and Contr. Fusion **47** (2005) B37.
[36]. Saarelma S. et al., Plasma Phys. and Contr. Fusion **49** (2007) 31.
[37]. Saarelma S. et al., Plasma Phys. and Contr. Fusion **47** (2005) 713.

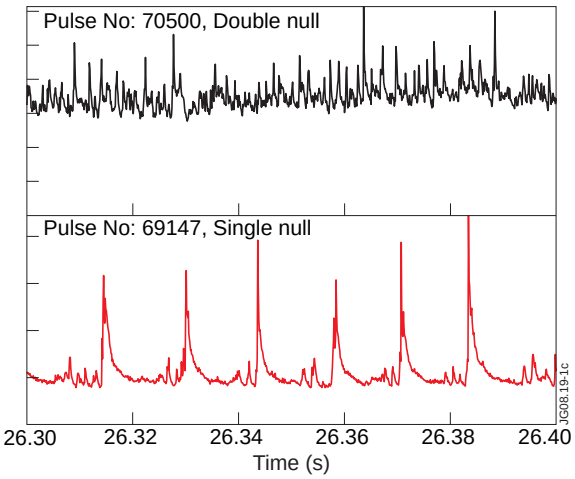

Figure 1: The D_α signal of a double null Pulse No: 70500 and a reference single null Pulse No: 69147.

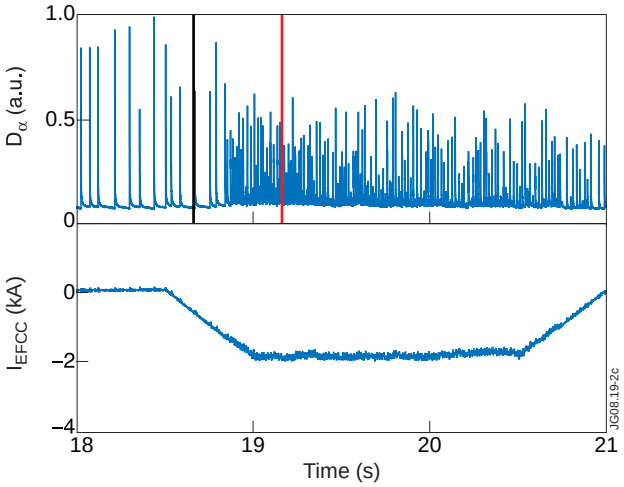

Figure 2: The D_α signal and the current in the error field correction coils in Pulse No: 69557. The vertical lines represent the timings of the HRTS laser pulses.

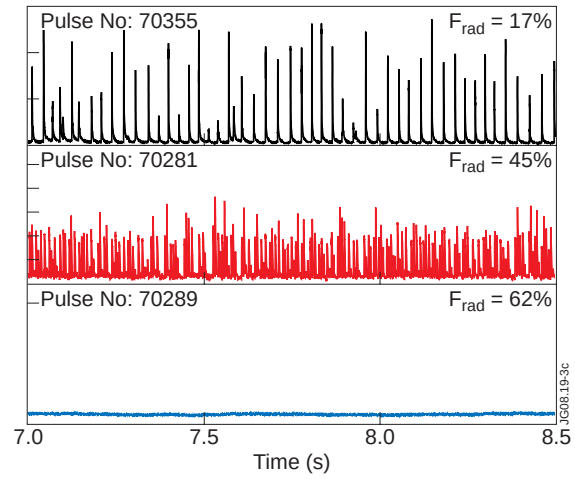

Figure 3: The D_α signal in the three different radiation regimes. The first plasma has Type I ELMs, the second Type III ELMs and the last one is in L-mode.

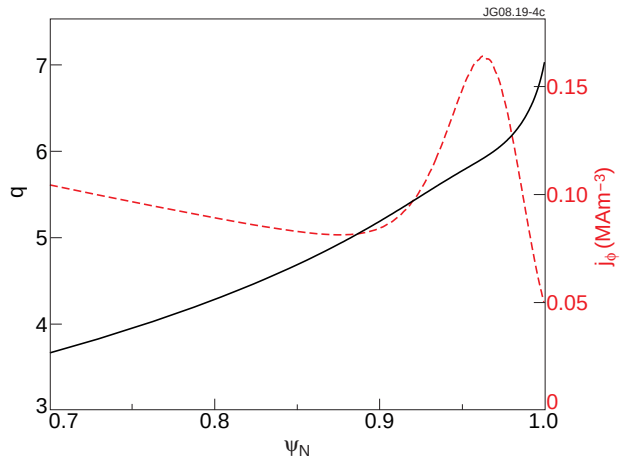

Figure 4: The flux surfaced averaged toroidal current density (red dashed line) and q-profile (black solid line) of a typical JET Type I ELMy plasma equilibrium.

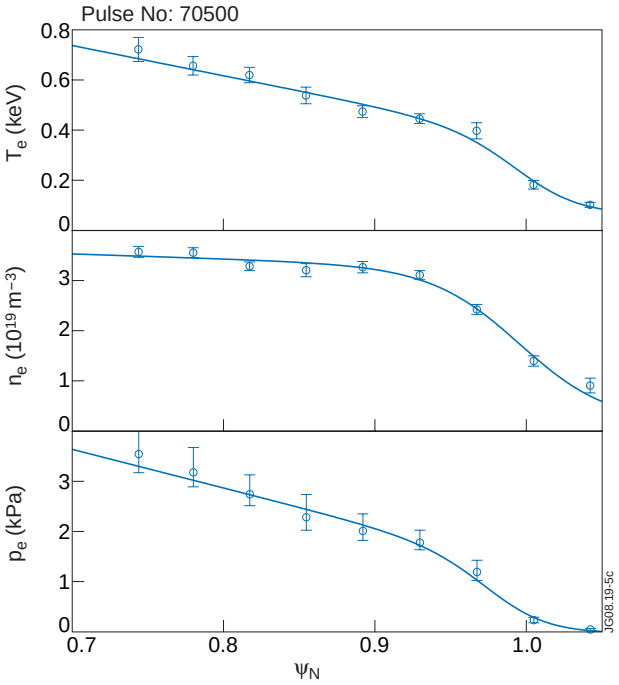

Figure 5: The HRTS electron temperature, density and pressure profiles in a Type II ELMy (Pulse No: 70500).

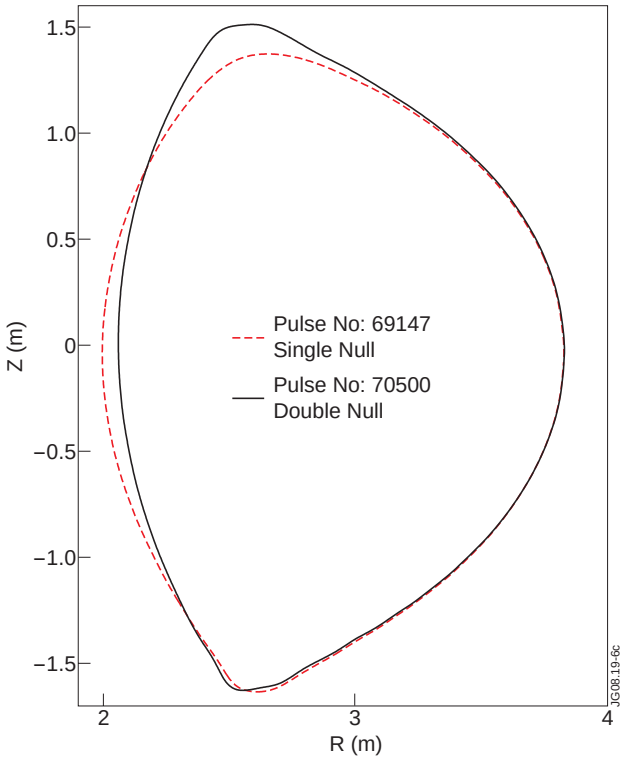

Figure 6: The plasma boundary shape for single null (Pulse No: 69147) and double null (Pulse No: 70500) discharges.

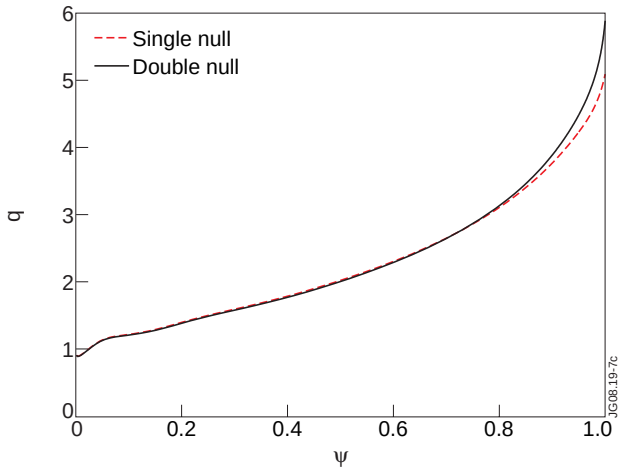

Figure 7: The q-profile of single and double null equilibria. Note that the plasma profiles are identical and the the only difference is in the boundary shape.

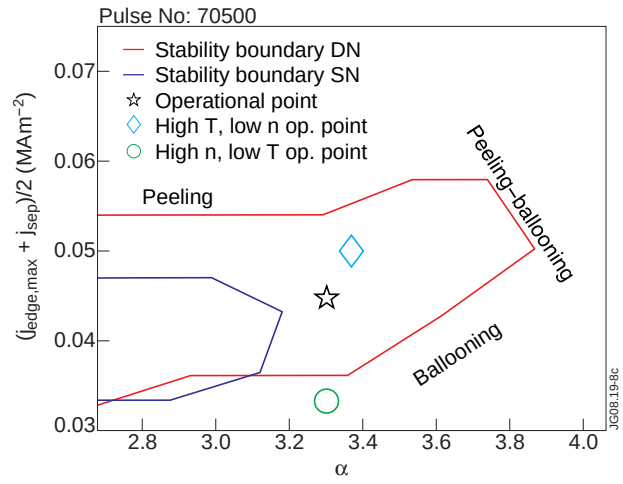

Figure 8: The edge stability boundaries for single and double null equilibria. The star (☆)shows the operational point for the experimental profiles from Pulse No: 70500 discharge at 65.288s. The diamond (◇) represents an equilibrium with increased pedestal temperature and decreased density and the circle (□) an equilibrium with decreased pedestal temperature and increased density.

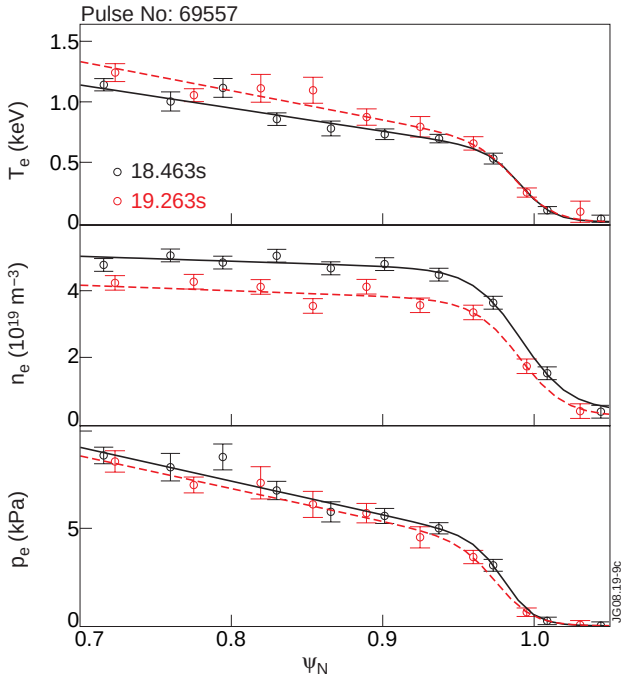

Figure 9: The electron density, temperature and pressure profiles before (18.463s) and during (19.263s) the ELM mitigation in Pulse No: 69557.

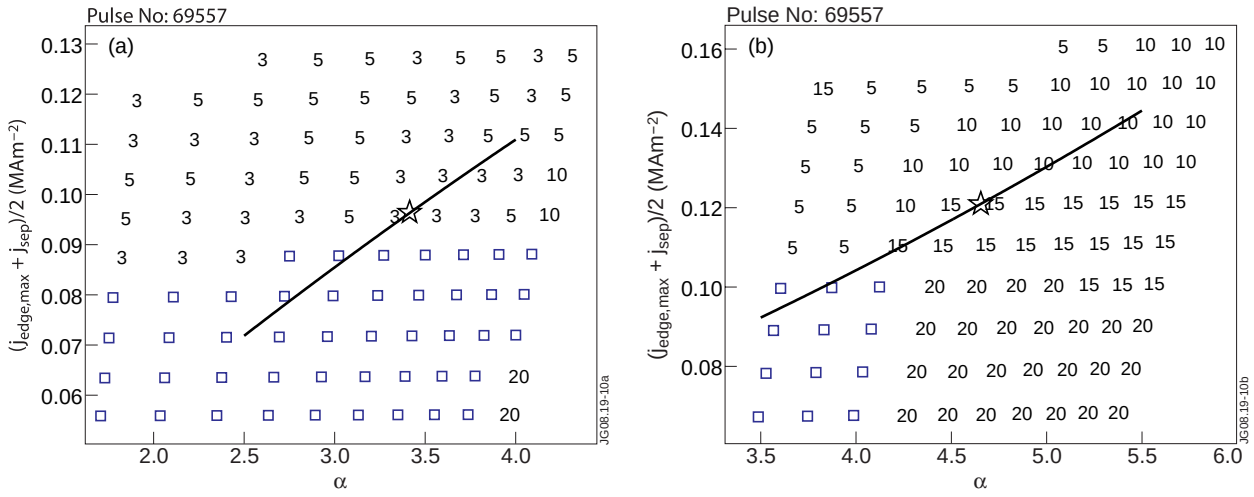

Figure 10: Edge stability diagrams of mitigated (a) and Type I ELMy (b) phase of the JET Pulse No: 69557. The stability is plotted for varying the maximum of the normalised edge pressure gradient (x-axis) and the current density (y-axis). The numbers show the toroidal number of the most unstable mode and the squares represent stable points. The black lines represent a self-consistent path for the experimental point across the stability boundary.

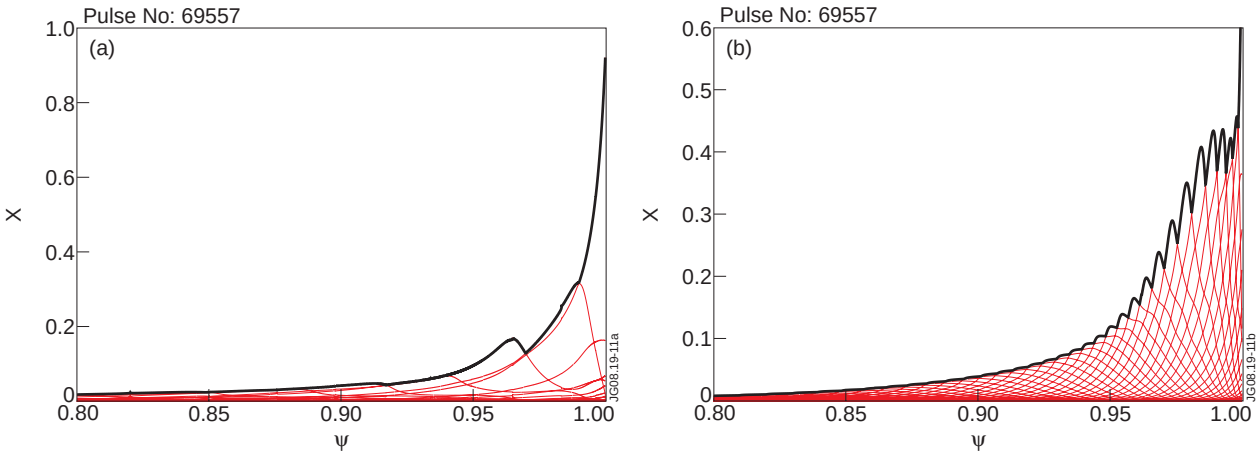

Figure 11: The radial mode structure of the most unstable mode in mitigated (a) and Type I ELMy (b) phase of the JET Pulse No: 69557. The toroidal mode numbers of the modes are n = 3 and n = 15, respectively. Each of the thin red lines represents a separate poloidal mode number (m) peaking at q = m/n. The thick black line shows the mode envelope.

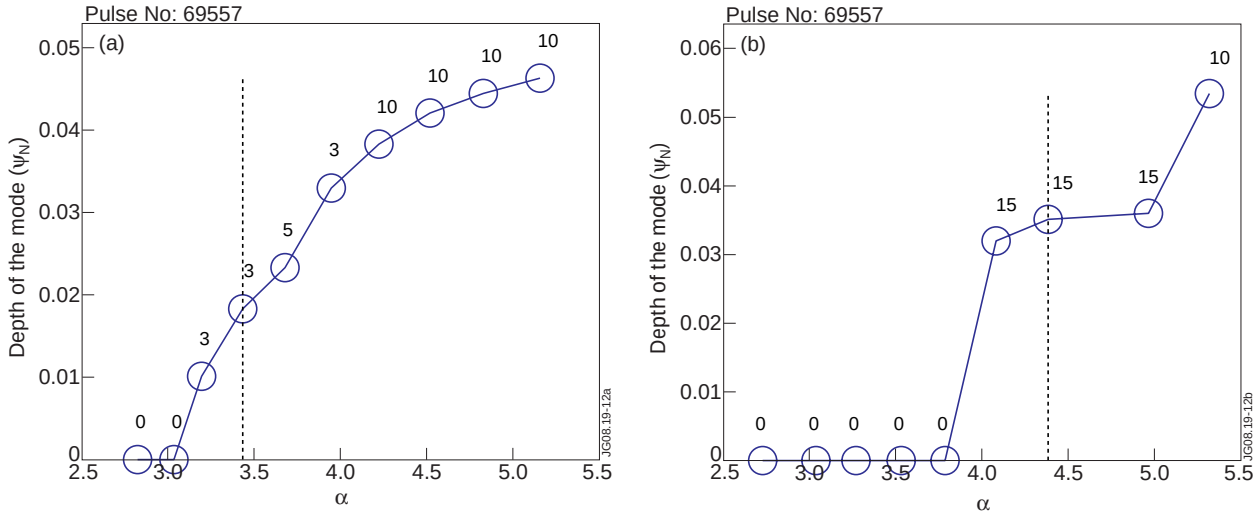

Figure 12: The width of the mode in mitigated (a) and Type I ELMy (b) phase of the JET Pulse No: 69557 along the path in Fig.10. The numbers represent the toroidal mode number of the most unstable mode. The vertical dashed line shows the position of the experimental point.

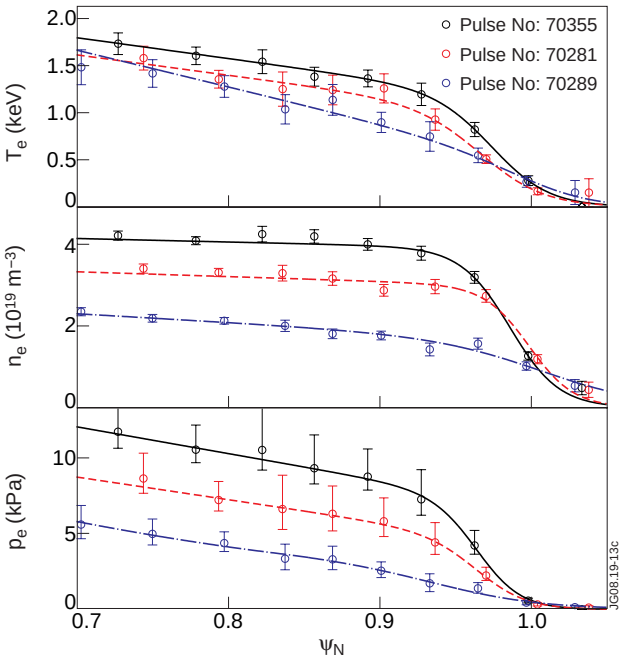

Figure 13: The HRTS electron temperature, density and pressure profiles in a Type I ELMy (Pulse No: 70355), Type III ELMy (Pulse No: 70281) and L-mode (Pulse No: 70289) discharges.

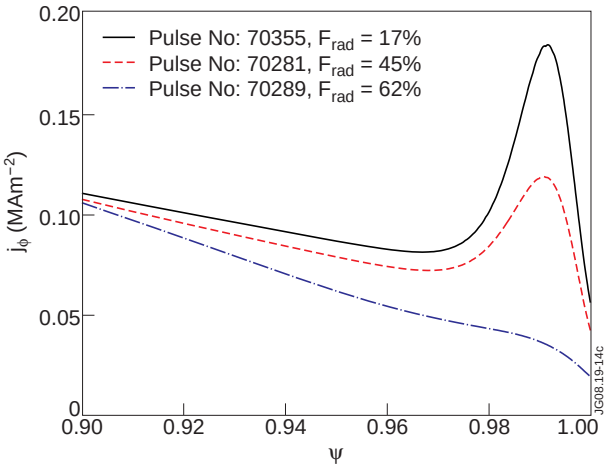

Figure 14: The calculated toroidal current density in the edge region for the three equilibria of F_{rad} = 17% (Pulse No: 70355, Type I ELMs), 45% (Pulse No: 70281, Type III ELMs) and 62% (Pulse No: 70289, L-mode).

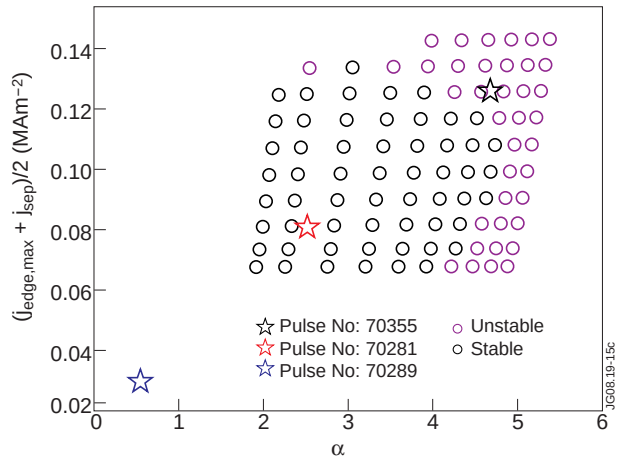

Figure 15: The stability diagram for three values of F_{rad} = 17% (Pulse No: 70355, Type I ELMs), 45% (Pulse No: 70281, Type III ELMs) and 62% (Pulse No: 70289, L-mode).